Ab initio studies of the (100), (110), and (111) surfaces of $CoSi_2$

R. Stadler and R. Podloucky
Institute for Physical Chemistry, University of Vienna, Liechtensteinstrasse 22A/1/3, A-1090 Vienna, Austria

G. Kresse and J. Hafner
Institute for Theoretical Physics, Technical University of Vienna, Wiedner Hauptstrasse 8-10/136, A-1040 Vienna, Austria

(Received 18 July 1997; revised manuscript received 20 October 1997)

Based on the ultrasoft pseudopotential technique of the Vienna *ab initio* simulation package, we performed *ab initio* calculations for the (100), (110), and (111) surfaces of $CoSi_2$ within the framework of the generalized gradient approximation. Surface energies were derived from the total energies as well as estimated from simple models. Relaxed surface geometries were determined for the (1×1) surfaces by force minimization. For the (100) surface a proposed $\sqrt{2}\times\sqrt{2}$ reconstruction was investigated that, however, is not stable. Energetical results as well as simulated scanning tunneling images strongly indicate that the reconstruction does not exist. The band structures show a number of surface states, in particular, in gaps of the projected bulk bands at and above Fermi energy for the (100) and (110) surface. For the Si-Co-Si terminated (111) surface, however, only two Si-like surface bands are found. Some surface states are analyzed in terms of density contours revealing covalent Co-Si bonding and coupling to deeper layers. Work functions are also provided. [S0163-1829(98)01307-1]

I. INTRODUCTION

$CoSi_2$ is of interest for the design of microelectronic devices[1] because it can be grown on Si or even forms buried layers in Si. Due to the small lattice mismatch, well-defined interfaces[2] of semiconducting Si to conducting $CoSi_2$ can be formed. The compound $CoSi_2$ has a low specific resistance at room temperature and provides a large mean free path of about 12 nm for the electrons. Therefore, $CoSi_2$ can be applied as the conducting part of metal-base and permeable-base transistors[3] and is set to replace $TiSi_2$ as primary silicide in CMOS devices in the future.

In particular the interfaces of $CoSi_2(100)/Si(100)$ and $CoSi_2(111)/Si(111)$ were experimentally studied.[4–7] In Ref. 4 a $\sqrt{2}\times\sqrt{2}$ reconstruction for the (100) surface is proposed on the basis of scanning tunneling microscopy data measured for epitaxially grown $CoSi_2$. However, more recent studies (e.g., Refs. 7–9) claim that the (100) surface is covered by Si adlayers because Co diffuses into the material.

Surprisingly, for the clean surfaces there are hardly any experimental data to be found, although for studying interfaces a profound knowledge of the clean surfaces is certainly of value. Furthermore, the strongly covalent bonding between Co and Si let one expect interesting surface states and related features. Also, there is only one extensive, very recent *ab initio* study of the clean (110) surface[10] available. Therefore, we believe it is important to investigate the structural, energetical and electronic structural properties of the most important $CoSi_2$ surfaces.

II. COMPUTATIONAL DETAILS

For all the calculations the Vienna *ab initio* simulation package[11] (VASP) was applied. VASP is based on the iterative diagonalization of the Kohn-Sham Hamiltonian in a plane wave basis using ultrasoft pseudopotentials according to Vanderbilt.[12,13] Because of the concept of augmentation charge densities this particular pseudopotential technique can also successfully be used for the treatment of, e.g., $3d$-transition metals, compounds[14] and their surfaces[15] and even for magnetic systems in a spinpolarized version.[16] Due to the augmentation correction formal complications arise, when compared to standard normconserving pseudopotential techniques. However, these disadvantages are by far outweighed by the substantial reduction in basis size and improved transferability of the pseudopotentials. Therefore, for our calculations a reasonably small energy cutoff of 200 eV yields converged results.

For the actual derivation of the ultrasoft pseudopotentials the atomic cutoff radii were 2.7 a.u. for Co (being the same for s, p, and d states), and 2.5 a.u. for Si (s and p states). The atomic configurations $3d^8 4s^1 4p^0$ for Co and $3s^2 3p^2$ for Si were chosen. Partial core corrections[17] were introduced to enable a proper treatment of the nonlinear dependence of the exchange correlation functional on the ground-state charge density. These choices yield reliable pseudopotentials which were tested in $CoSi_2$ bulk studies.[14]

The **k** points in the irreducible part of the Brillouin zone (IBZ) were constructed according to a special **k**-point technique.[18,19] The number of **k** points was considered to be converged when the atomic relaxations were varying by less than 0.01 Å.

By using Monkhorst's scheme[18] a $7\times7\times1$-grid was used resulting in 10, 16, and 8 **k** points in the irreducible part of the Brillouin zone for the (100), (110), and (111) surfaces, correspondingly. Furthermore, a $5\times5\times1$ grid was designed for the more expensive reconstruction study of the (100) surface yielding 6 **k** vectors in the IBZ. For the bulk reference, a $7\times7\times7$ grid was constructed, which corresponds to 44 **k** points in the IBZ. All VASP calculations were performed within the framework of the generalized gradient approximation (GGA) of Becke and Perdew[20] because of the good

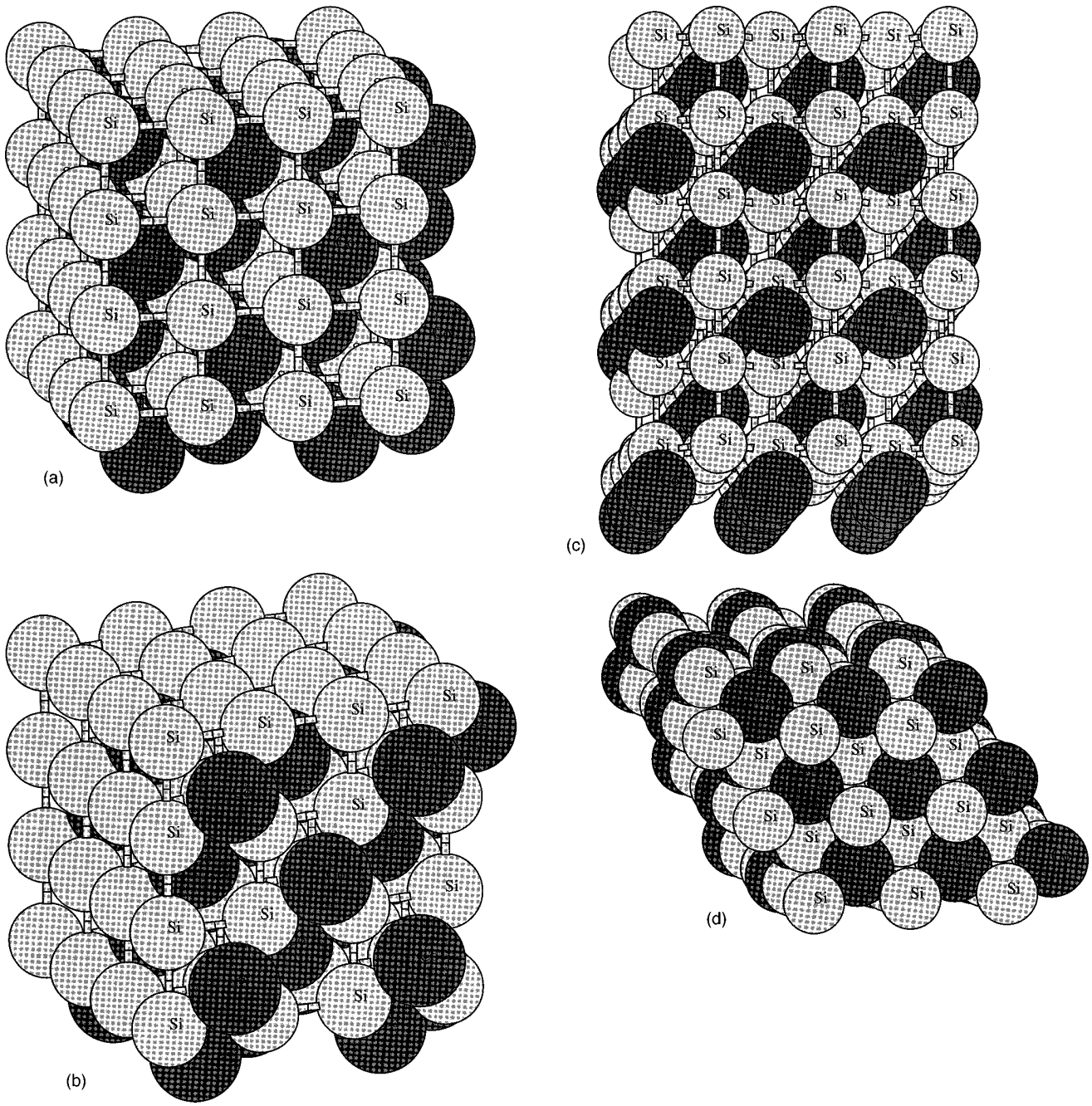

FIG. 1. Top view of the atomic arrangements for the clean (100), (110), and (111) surfaces of $CoSi_2$: (a) (100) Si terminated, b) (100) Co terminated, (c) (110), (d) (111).

agreement with experimental data for bulk properties.[14] Therefore, the calculated bulk equilibrium lattice spacing of 5.350 Å was taken for the present calculations using GGA. In addition, LDA calculations were performed at the experimental bulk lattice parameter of 5.365 Å. Relaxation of the atomic positions of the two topmost layers was achieved by force minimization.

Threedimensionally periodic slabs with proper size of the vacuum region were constructed for the surface studies. The chosen thicknesses of the slabs for the (1×1) calculations of the (100), (110), and (111) surface corresponds to seven stoichiometric $CoSi_2$ units according to the proper stacking sequence. In order to study a proposed $\sqrt{2}\times\sqrt{2}$ reconstruction of the (100) surface, the corresponding slab was doubled in size in the surface plane. For preliminary studies of adlayers on the (100) surface, a smaller slab of two $CoSi_2$ units plus unrelaxed adlayers in two possible hollow positions was constructed.

Figure 1 shows top views of the three surfaces under study. Because we preferred to choose the proper bulk stackings with stoichiometric $CoSi_2$ units, the slab for the (100) case has two different surfaces [Figs. 1(a) and 1(b)]. The (110) slab consists of stoichiometric $CoSi_2$ layers with just one type of surface [Fig. 1(c)]. As discussed in the paper for the (111) surface, two different terminations would be possible. However, as a result from our calculations as well as from experimental findings,[7] the Si-Co-Si termination [Fig. 1(d)] is the stable and most interesting one.

Due to the polar nature of the (100) slab and the repeated-slab construction one has to take into account artificial dipole-dipole interactions in the direction of the surface normal. From test calculations deriving the dipole moment of the slab it was found that for a vacuum region of 6 bulk spacings the dipole-dipole energy was negligibly small ($\leqslant 1$ μeV). The precision of the calculation of the dipole moment was checked by calculating the dipole moments of hydrogen-halogenide molecules, for which we found excellent agreement with experiment.[21] We also studied the dependency of surface relaxations on the size of the vacuum region which was chosen sufficiently large, so that the Si-terminated surface is decoupled from the Co-terminated one across the vacuum.

III. STRUCTURE AND ENERGETICS

A. Surface energetics

The (100), (110), and (111) surfaces were modeled by slabs of perfect $CoSi_2$ stoichiometry and proper stacking in order to avoid problems with stacking faults and definitions of surface energies (or cleavage energies, rather). Cleaving a single crystal of a compound leads to two surfaces that, depending on the orientation of the cleaving plane, are different concerning the compositions or geometry of the surface layers. This is the case for $CoSi_2$ (100), because cleaving produces a Co terminated and a Si_2 terminated block [Figs. 1(a) and 1(b)]. The cleavage energy G_c can be written as

$$G_c = \gamma_1 + \gamma_2, \tag{1}$$

being the sum of two different surface energies γ_1 and γ_2. In general, the surface energies cannot be obtained for each surface separately.

For slab calculations, G_c can be directly evaluated from the difference of the total energy $E_{\mathrm{slab}}(n_u)$ for a slab with n_u stoichiometric units stacked properly along the surface normal, and the total energy of the corresponding bulk reference E_{bulk},

$$G_c(\mathrm{slab}) = E_{\mathrm{slab}}(n_u) - n_u E_{\mathrm{bulk}}. \tag{2}$$

For the symmetric (110) surface of $CoSi_2$ [Fig. 1(c)], the surface energy is uniquely defined by $\gamma = G_c/2$. For the (111) surface, the stoichiometric stacking unit consists of one Co and two different Si planes, offering now two different cleavage planes [Fig. 1(d)], namely, (i) either between two Si planes or (ii) separating a Co-terminated block from a block terminated by two Si layers. Termination (i) consists of a trilayer termination Si-Co-Si with one Si layer on top, and yields two identical surfaces of the slab. The second termination (ii) will result in a slab with two different surfaces, namely, one with two terminating Si layers, and the other one consisting of a pure Co layer. Experimentally, it seems now clear (Refs. 22–25) that termination (i) is preferred for the clean (111) surface. In accordance with these experimental findings from our calculated cleavage energies we learn that termination (ii) is much more costly because of $G_c(ii) \approx 2 \times G_c(i)$ for the cleavage energies of the corresponding terminations. For that reasons, all following discussions for $CoSi_2$(111) refer to the case of the Si-Co-Si termination. Care must be taken when experimental data for (111) surfaces are considered, because in most cases measurements were done on surfaces with additional Si adlayers, e.g., in Ref. 6.

TABLE I. Calculated cleavage energies $G_c = \gamma_1 + \gamma_2$ (J m^{-2}) for $CoSi_2$ per surface area. Quantities γ_1, γ_2 denote surface energies of both surfaces of corresponding stoichiometric slabs. Results of LDA and GGA calculations for bulk-terminated atomic positions (bulk), and GGA values for relaxed geometries (relax). Surface area A in units of bulk lattice parameter a_0^2.

		LDA	GGA	
	A	G_c(bulk)	G_c(bulk)	G_c(relax)
100	1/2	5.96	4.13	4.02
110	$1/\sqrt{2}$	4.62	2.94	2.87
111	$\sqrt{3}/4$	4.34	2.18	1.96

Table I shows cleavage energies for the three main orientations derived from local-density approximation (LDA) and generalized gradient approximation (GGA) calculations. As it is customary, the given values are actually energies per surface area, the size of the area varying according to the table. The values of G_c for the (100) surface are the largest ones, and the data for (111) the smallest. Obviously, the LDA-derived results are substantially larger than the GGA values [e.g., for (111) more than a factor of 2] demonstrating the LDA effect of stronger binding compared to the GGA. Furthermore, GGA yields much larger differences of G_c for the (110) and (111) surfaces. The LDA value for the (110) case is about 0.2 eV larger than the result of a very recent *ab initio* study based on the full-potential linearized augmented plane-wave method (FLAPW).[10] Such a difference of cleavage energies might be due to the applied two different **k**-space sampling methods although results for bulk $CoSi_2$ were in excellent agreement.[14] In the latter study, however, all numerical parameters could be absolutely converged, which—due to the computational costs—is not the case for the surface studies. In our present study, E_{bulk} was derived from bulk calculations with the same stacking as the corresponding slab for the surface.

Relaxation of surface geometries (last column of Table I) leads to a reduction of G_c by 0.11, 0.07, and 0.22 J m^{-2} for the (100), (110), and (111) surfaces, correspondingly. For the (100) surface, the relaxation of the Co-terminated surface of 0.09 J m^{-2} dominates the relaxation of the Si-terminated case. For the (111) orientation, the relaxation energy is by far the largest because the Si surface layer is strongly pulled inwards by 0.16 Å (see Table IV).

$CoSi_2$ is considered to be a material with distinct covalent bonding as is also plausible studying the bulk density of states[10] in which bonding and antibonding features are distinctly separated, creating a pseudogap about 1 eV above the Fermi energy. Because of that property, one might be tempted to describe the cleaving process in terms of breaking bonds.

For that purpose, we apply a simple model by breaking up the corresponding bulk total energies in bond energies acting between the nearest-neighbor atoms. First, the CaF_2 crystal structure of $CoSi_2$ is decomposed into three fcc lattices, the Co and Si_1, Si_2 sublattices with the lattice parameter of bulk $CoSi_2$. We define now the energy per Co-Co bond and per

TABLE II. Lengths d_{AB} in Å and energies E_{AB} in eV for nearest-neighbor bonds between atoms A and B for $CoSi_2$. E_{AB} is derived from cohesion energies and energies of formation as described in the text. Results of GGA and LDA calculations. Si_1, Si_2 refer to different fcc Si sublattices. Last four columns: nearest-neighbor bulk coordination C, and numbers of broken bonds for the given surface orientation. For each of the two Si sublattices there are 12 bonds. The considered (111) surface is generated by cleaving the crystal between two Si layers.

Bond		GGA	LDA		Broken bonds		
A-B	d_{AB}	E_{AB}	E_{AB}	C	100	110	111
Co-Si	2.32	0.83	1.02	8	4	2	1
Si_1-Si_2	2.68	0.63	0.70	6	2	4	3
Si_1-Si_1	3.78	0.34	0.43	2×12	8	12	6
Co-Co	3.78	0.17	0.23	12	4	6	3

Si_1-Si_1, Si_2-Si_2 bond by the corresponding cohesive energies divided by 6 because of the fcc coordination of 12 nearest neighbors.

In the next step, the two Si sublattices are put together spanning the Si_2 lattice with empty Co sites. We assume now that the gain in binding energy is exclusively due to the formation of Si_1-Si_2 bonds without any change of energies of the already existing bonds. Then, the bond energy of Si_1-Si_2 is the formation energy divided by 6, the number of nearest neighbors in the Si_1-Si_2 lattice. Finally, Co is added to Si_2, and by assuming that all energy gain is due to the formation of the newly formed Co-Si bonds, the energy of these bonds is derived from the corresponding formation energy now divided by 8, because Co is in the center of a cube of Si atoms. Following this prescription, the bond energies of Table II are obtained from *ab initio* total energies of LDA and GGA calculations. Table II reveals that comparable in strength to the shortest and strongest bond, the Co-Si bond, is the Si_1-Si_2 bond. The longer $Si_{1,2}$-$Si_{1,2}$ bonds of the fcc sublattices are weaker by about a factor of 2. The Co-Co bond strength is rather small because the corresponding bond length is stretched by about a factor 1.6 compared to the Co-Co distances of its fcc bulk ground state.[14]

Table II lists the numbers of bonds n_{AB} broken by the cleavage process together with the bond energies E_{AB} derived from cohesive energies and energies of formation. If we assume the simplest possible model that the cleavage energy G_c(bond) is given by the number of broken bonds and the unchanged bond energies,

$$G_c(\text{bond}) = \sum_{AB} n_{AB} E_{AB}, \tag{3}$$

then we obtain values that are larger by a factor of 2 compared to the values of the column ''bond'' in Table III. However, as extensively studied by Methfessel *et al.*[26] for surfaces of $4d$-transition metals, the energies of the breaking bonds are reduced when the coordination number C is changed. Then for larger values of C, effective bond strengths $E_{AB}^{\text{eff}} \approx 1/2 E_{AB}$ should be inserted in Eq. (3). Applying this prescription the values for G_c^{eff}(bond) in Table III were derived.

TABLE III. Cleavage energies in eV of $CoSi_2$. Calculated for the unrelaxed slabs [G_c(slab)], from broken bulk bonds [G_c^{eff}(bond)], and as the difference of cohesive energies of monounits and bulk [G_c(mono)]. For further details, see text. All values are derived from GGA results and for the bulk lattice parameter of 5.350 Å.

	Slab	Bond	Mono
100	3.69	4.00	3.84
110	3.71	4.66	4.46
111	1.69	2.64	2.13

Table III compares G_c^{eff}(bond) to the cleavage energies G_c(slab) derived from slab calculations. These values are now not divided by the surface area. The values of G_c(slab) for the (100) and (110) slab are rather similar. The value for (111), however, is substantially lower. Apart from the actual size, a comparable sequence of values is found for G_c^{eff}(bond), which—by construction according to Eq. (3)—are interpreted easily: for both, the (100) and (110) surface, the sum of the strong Co-Si and Si_1-Si_2 broken bonds is $n_{AB}=6$, and, therefore, the cleavage energies are closer to each other than to the value for the (111) surface. Inspecting the (111) surface much less bonds are broken, in particular, only one Co-Si bond, and therefore much less energy is lost. Compared to G_c(slab) the cleavage energies G_c^{eff}(bond) are larger by 0.3–1 eV, and the values for the (100) and (110) surface are different by 0.7 eV. Having in mind the rather complex bonding of the $CoSi_2$ compound (three different nearest neighbor environments and two different types of atoms) when compared to the simple situation of $4d$-transition metals, the receipe of Methfessel *et al.* seems reasonable. Even some refinement might be possible [Eq. (3c) of Ref. 26], which requires some trend studies. However, in contrast to the procedure of Ref. 26, which recommends the non-spin-polarized atomic ground state for the free atoms as a reference for the cohesive energies, we have taken into account the spin-polarized atomic energies. Our argument is that because of the substantial gain in spin-polarization energy of 1.29 eV for the free Co atom, the Co-Co bond energy of 0.17 eV (Table II) is much lower than the one derived from the cohesive energy with a nonmagnetic atom as a reference; consequently, the values for G_c^{eff}(bond) would then be even larger. Spin polarization of the Si atom is of lesser influence because of the smaller spin-polarization energy gain of 0.75 eV. The remaining bond energies for Co-Si and Si_1-Si_2 are derived from formation energies based on nonmagnetic bulk phases. Therefore, they are not influenced by atomic ground states.

A further model for the cleavage energy was constructed by deriving the cohesive energies of the stoichiometric $CoSi_2$ monounits, which—when properly stacked—build up the slabs, consisting of two, one, and three layers for the (100), (110), and (111) orientations, respectively.

By taking the difference of cohesive energies of monounits and the bulk reference of $E_{\text{coh}}(\text{bulk}) = 18.29$ eV, we derive a cleavage energy G_c(mono) by

$$G_c(\text{mono}) = E_{\text{coh}}(\text{mono}) - E_{\text{coh}}(\text{bulk}). \tag{4}$$

TABLE IV. Relaxations in Å of atomic positions in the surface-(S) and subsurface-($S-1$) layers for $CoSi_2$ surfaces of (1×1) geometry. Experimental data from (a) Ref. 5 and (b) Ref. 6. (100)-Co for Co-terminated and (100)-Si for Si-terminated (100) surface.

			GGA-Calc.		Expt. (a)	Expt. (b)
	layer	atom	Δy	Δz	Δz	Δz
100-Co	(S)	Co		-0.08		
	(S-1)	Si		$+0.01$		
100-Si	(S)	Si		-0.04		
	(S-1)	Co		$+0.03$		
110	(S)	Co		-0.04		
		Si	±0.02	-0.09		
	(S-1)	Co		-0.01		
		Si	±0.01	$+0.01$		
111	(S)	Si		-0.16	-0.11	-0.13
	(S-1)	Co		-0.06	0.0	-0.02

According to Table III the energies G_c(mono) already reflect the trend of the actual surface energies and they are closer to the values for G_c(slab) than the results for G_c(bond). The substantially smaller G_c(mono) for the (111) unit means that its corresponding atomic arrangment (a Si-Co-Si trilayer with a hexagonal two-dimensional lattice) is significantly more stable than in the other monounits. Searching the energy minimum as a function of the in-plane lattice spacing lowers the total energies by 0.4–0.5 eV for (100) and (110) monounits, whereas the gain for the (111) unit is only 0.1 eV.

B. Geometry and relaxations

1. (100)

For the unreconstructed but relaxed (1×1) surface of our study (Table IV), we obtained quite different contractions Δz of the first layer spacings of -0.08 Å for the Co-terminated surface, and -0.04 Å for the Si_2-terminated surface. For the next interlayer spacings only small, now positive changes of $+0.01$–0.03 Å are found. All other Δz values are negligible, since the perturbation due to the surface is dying away rapidly.

Based on scanning tunneling microscopy (STM) data Stalder *et al.*[4] claimed a $\sqrt{2}\times\sqrt{2}$ reconstruction for the clean surface, which is usually called the C surface. It should be noted that the denomination of C surface and S surface is somewhat misleading: the C surface is terminated not by Co but by one layer of Si_2, whereas the so-called S surface[4] is covered by an additional layer of Si atoms on top of the C surface.

The interpretation of the STM data is that the squares of Si surface atoms are contracted towards the corresponding hollow positions above empty sites of the Co subsurface. This contraction should be due to dangling Si bonds leading to an accumulation of charge in the center of the now contracted squares being partially saturated in this process and thus increasing the tunneling current. From our calculations we could neither find the proposed reconstruction nor corroborate the proposed STM images. The results of the STM simulation will be discussed in Sec. III C.

For the reconstruction study we designed a suitable supercell with $\sqrt{2}\times\sqrt{2}$ periodicity. Surface atoms were relaxed statically after the squares of Si atoms were contracted as much as 0.23 Å along the diagonal of the squares. In all cases searching for the minimum of forces, the atoms always moved back to their original positions of high symmetry. Simple model studies for much larger contractions were also made for Si_2 monolayers, and slabs consisting of one and two $CoSi_2$ units. In all cases no stabilizing effect could be achieved by contracting the Si squares. In the monolayer case, however, we found that for contractions in the range of 0.15–0.25 Å the total energy remained rather constant, but increased again for larger contractions. That was the reason why—for the large slab system—such large distortions were considered. Based on a simple argument, the proposed contraction and reconstruction would be surprising, because the original quadratic Si lattice is of such high symmetry that—without any additional perturbations such as adsorbates—one would expect a large energy cost for any distortion of the squares.

The experiments were performed on $CoSi_2$ epitaxially grown on Si at room temperature, and it is claimed that $CoSi_2$ forms a complex terrace structure. However, the area of terraces is reported to be quite large (1000×1000 Å^2) so it should represent a single-crystal surface. Epitaxial layers with various thicknesses up to 105 Å have been grown on the Si templates. Therefore, the influence of the Si substrate on the $CoSi_2$ surface should be negligible. In addition, the lattice mismatch is rather small.

It could, however, be the case that adlayers of Si were present because according to the experimental study of Ref. 6 the (100) C surfaces were always covered by Si adlayers. A number of experiments were made for $CoSi_2$(100) films on Si(100) or $CoSi_2$(100) bulk-terminated phases with Si adlayers. One of the most recent works applying low-energy electron diffraction[7] (LEED) studied Si adlayers on the $CoSi_2$(100) bulk-terminated surface, proposing a $c(2\times2)$ arrangement for the Si-adlayer atom in hollow positions. Analyzing the LEED data for the change of interlayer spacings with respect to the bulk distance, the authors found rather strong oscillations with amplitudes of 0.15–0.20 Å and an expansion for the spacing between the surface Si_2 layer and the adatoms. The rather large oscillations according to the analysis of the LEED data must then be caused by the Si adlayer, which seems to also impose a more long-ranged coupling between the layers in contrast to our results for the clean surface.

2. (110)

The (110) surface has so far not been investigated experimentally. According to Table IV, the surface Co and Si atoms are pulled inwards, but in a different way leading to a rumpling of 0.05 Å with Co as the topmost atoms. Due to the symmetry of the (110) surface the Si atoms are free to change one lateral coordinate but this kind of reconstruction is rather small. The relaxations in the subsurface layers are

nearly negligible. An LDA calculation was also done resulting in relaxation geometries and energy in very good agreement with FLAPW data.[10]

3. (111)

Experimental data are available for the clean (111) surface that—as discussed in the last section—is terminated by a Si-Co-Si trilayer. The experiments referred to in Table IV agree very well with our results concerning the strong inwards relaxation of the top Si layer. The amount of this relaxation is about two times larger than for the other two directions presumably because the dangling Si orbitals are strongly attracted towards the Co of the subsurface. Due to the local environment provided by the (111) stacking, for the surface Si atoms Co may act as a substitute for the missing Si atoms [see Fig. 1(c)]. According to our calculation, also the Co subsurface layer experiences a still nonnegligible inwards relaxation which was not observed by experiment. However, one has to take into account the error margins of the low-energy electron diffraction experiments.

C. STM simulation for the (100) surface

As discussed previously Stalder *et al.*[4] interpreted their experimental data in terms of a $\sqrt{2}\times\sqrt{2}$ reconstruction of the clean (100) surface. Based on the *ab initio* electronic structure we can simulate STM images and derive corrugation heights. We do this by relying on the model of Tersoff and Hamann[27] in which the two-dimensional STM intensity is related to the contour lines of the local density of states (LDOS) integrated over the energy range of $E_F \pm \Delta E/2$. The energy range $\Delta E/2$ is fixed by the potential to be 20 meV according to the experiment. The properly weighted and energy integrated LDOS $g(\mathbf{r},\Delta E)$ is now given by

$$g(\mathbf{r},\Delta E)=\sum_{\mathbf{k},n}^{\Delta E} |\psi_{\mathbf{k},n}(\mathbf{r})|^2 f(\epsilon_{\mathbf{k},n}-\epsilon_F)[1-f(\epsilon_{\mathbf{k},n}-\epsilon_F)], \tag{5}$$

summing over the Kohn-Sham orbitals $\psi_{\mathbf{k},n}$ with band index n and $\mathbf{k}$ vectors of the Brillouin zone. Only such states are taken into account which are in the allowed energy range. To account for finite temperatures the LDOS is weighted by a Fermi function $f(\epsilon-\epsilon_F)$ corresponding to 293 K in our case. The tip is treated, correspondingly, by the function $1-f$. The calculated images are a logarithmic representation of the function $g(\mathbf{r},\Delta E)$.

What is needed further, is the distance between the tip and the atoms of the surface. We estimated it by using an inverse decay length of $\kappa=16.5\ \mathrm{nm}^{-1}$ and the relation for the Ohmic resistance of $R=h/2e^2\times e^{\kappa z}$, which resulted in a core-core distance of $z\sim 1.4$ Å. By adding the atomic radius of Si of 2.19 Å, finally the tip-substrate distance of 3.6 Å was derived. The applied inverse decay length was taken from Biedermann[28] who derived the value from experimental STM scans for Fe(100). Since—to our knowledge—no other values for κ are known, we had to rely on that. Although it is rather difficult to derive the experimental tip-sample distance, it is of importance to know, because the calculated images might be sensitive to this parameter.

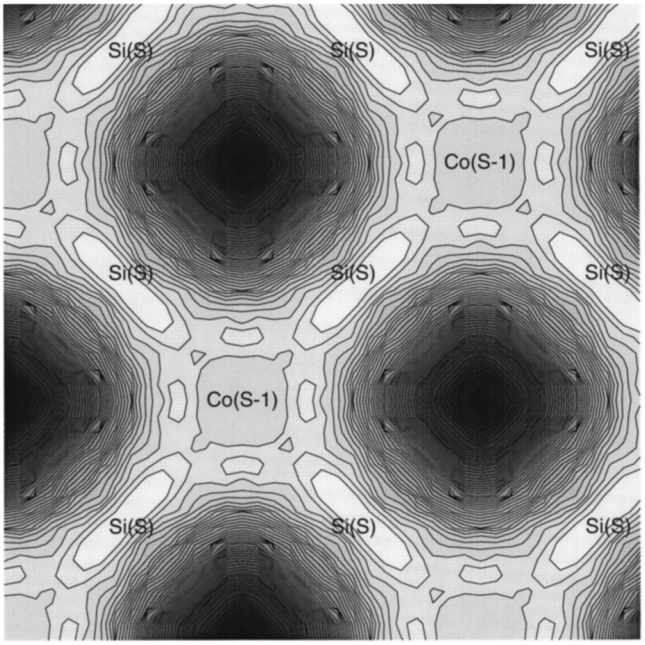

FIG. 2. Contour plot of a simulated STM image for unreconstructed (100) surface of $CoSi_2$ where bright area marks the maxima in tunneling current intensity and dark area the minima. The cut parallel to the surface was made in a distance of 3.6 Å above the Si surface positions. The x and y axes are in the [010] and [001] directions. Si surface layer: Si(S), Co subsurface layer: Co ($S-1$). Logarithmic scaling for contours. Further details described in the text.

Figure 2 shows a calculated STM image for the (1×1) unreconstructed surface at a tip height of 3.6 Å. The regions of higher LDOS form a networklike pattern with its maximum at the surface Si positions, being also fairly large at the positions above the Co subsurface positions. The basic features are quite similar to the image of the artificially reconstructed (100) surface in Fig. 3. Maximum-intensity features are now found around positions above the subsurface Co atom and not at Si sites. Again, a network pattern is formed without any resemblance to the experimental data of Stalder *et al.*,[4] in which the maximum features form square-shaped spots. It is proposed that these will arise in hollow positions, underneath which their is no Co atom. Our images are totally different from the results of Ref. 4.

To study the influence of the tip-sample distance we varied the tip height for the unreconstructed case from 3 to 4 Å. We observed that for distances smaller than $\approx$3.7 Å the images are rather similar to Fig. 2, apart from increasing the weight of the oval-shaped features above the Si atom, when reducing the distance. Moving the tip to distances larger than 3.7 Å, the LDOS above the Co positions increases forming rather localized spherical spots.

Recently it was claimed[6] that (100) surfaces are always covered by Si adlayers, so there are no stable C surfaces but only S surfaces. Therefore, we also performed simplified model calculations for such adlayers by covering 50% of the surface described in Sec. II. Two different adsorption sites were studied: Si in a hollow position above empty Co-subsurface sites (suggested by Starke *et al.*[6]), and Si at the second possible hollow sites. For both types of adlayer adsorption, a $\sqrt{2}\times\sqrt{2}$ structure is formed. No relaxation of the

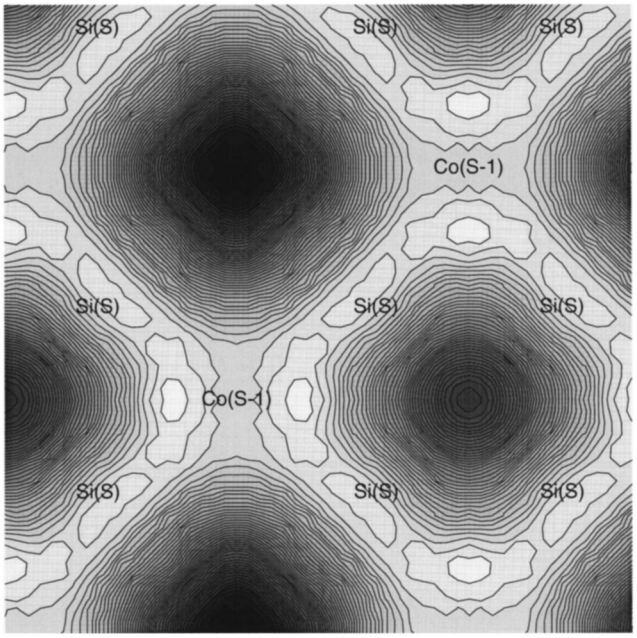

FIG. 3. Contour plot of a simulated STM image for the artificially reconstructed (100) surface of $CoSi_2$. Reconstruction: Si-Si squares contracted by 0.23 Å along the diagonals. For details see Fig. 2.

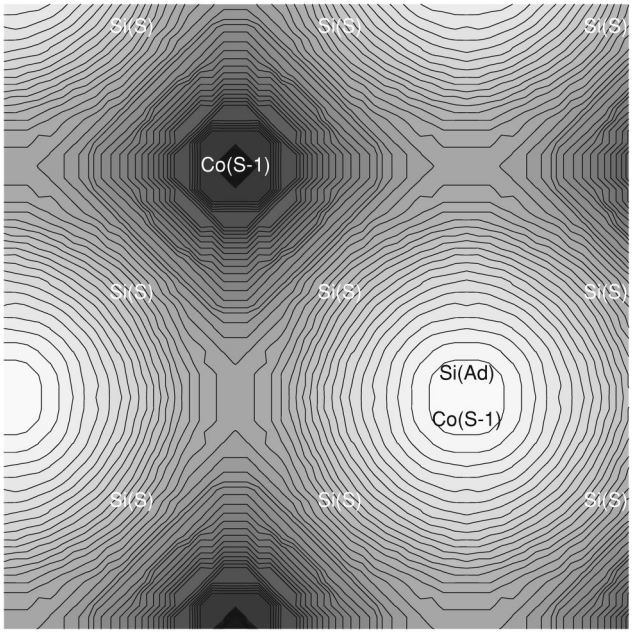

FIG. 5. Contour plot of a simulated STM image for the unreconstructed (100) surface of $CoSi_2$ covered by a $\sqrt{2}\times\sqrt{2}$ adlayer of Si. Adlayer positions above Co sites. For details see Fig. 2.

adatoms was calculated; therefore, the results are only preliminary ones. However, the Figs. 4 and 5 clearly show that now the maximum of the image is at the adlayer position. The result for the proposed adlayer coverage (Fig. 4) is very similar to the STM scans of Stalder *et al.* with deep holes, intermediate saddles above the Co-subsurface places, and the bright round peak above the Si adlayer. The result for the other geometry (Fig. 5) shows less pronounced variations. From all that, we conclude that the measurements of Stalder *et al.* were done on a (100) surface with Si-adlayer atoms, and the proposed reconstruction of the clean surface does not exist.

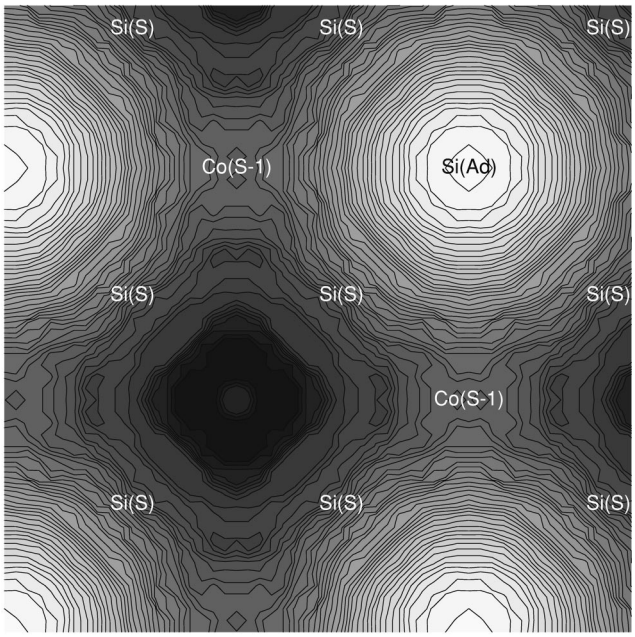

FIG. 4. Contour plot of a simulated STM image for the unreconstructed (100) surface of $CoSi_2$ covered by a $\sqrt{2}\times\sqrt{2}$ adlayer of Si. Adlayer positions above hollow sites (empty Co sites). For details see Fig. 2.

We also derived the corrugation heights according to Ref. 29 for the STM images of Figs. 2, 3, and 4, which are defined as the difference in height between the maximum and minimum of the LDOS. In their experimental data Stalder *et al.* found a difference in corrugation heights for the two structural features, the bright spots and the gridlines, being about 300 m Å. On the basis of our images we obtained 80 m Å for the unreconstructed and 120 m Å for the reconstructed clean surface in our calculations. One can expect[29] that within the model of Tersoff and Hamman the corrugations could be smaller by about a factor of 2 compared to experiment. However, the found discrepancy seems to be too large to claim any agreement between our calculations and the STM experiment. For the suggested adlayer structure of Fig. 4 we derived a corrugation height difference of 300 m Å, which would be in perfect agreement with experiment. It should be noted that this value is based on a simplified model with a rather small number of $CoSi_2$ layers and—what might be more important—the positions of the Si-adlayer atoms are not relaxed. Nevertheless, it can be expected from the data that the adlayer geometry will result in a substantially higher in-plane variation of the corrugation than for the clean surface.

Recently, Voigtländer *et al.*[30] performed FLAPW calculations on adlayer systems corresponding to the *S*-surface type of the $CoSi_2(100)$ surface. In contrast to our work, the adlayer was modeled by occupying half of the positions by Co. It was argued that inhomogeneous occupation of lattice sites could be responsible for the observed distinct voltage dependence of the tunneling current.

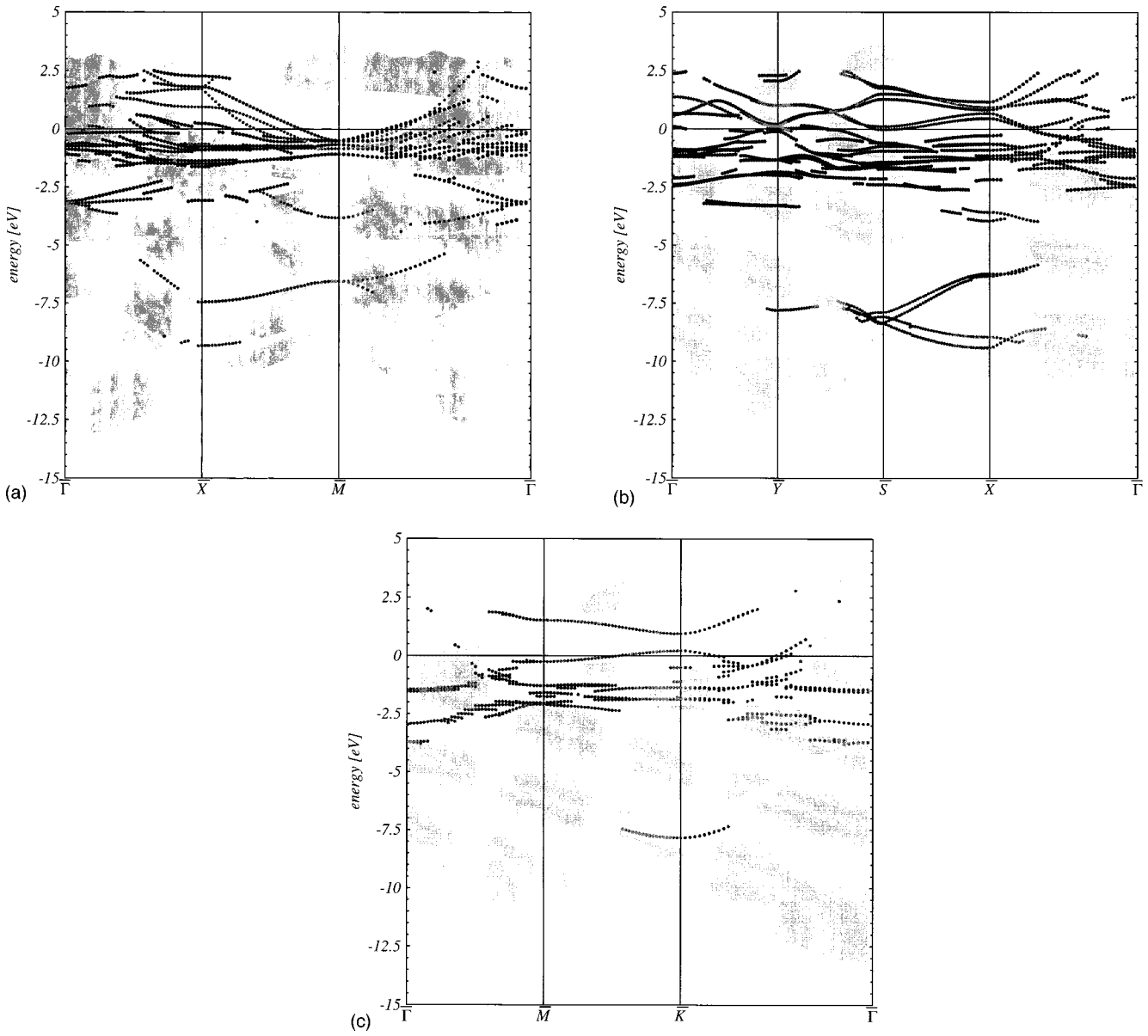

FIG. 6. Energy bands for the (a) (100), (b) (110), and (c) (111) surfaces. Definition of surface localized states according to localization in surface atomic spheres; for details see text. Surface state of Co character, black dots; Si-character, gray dots. Bulk projected bands, shaded area.

IV. SURFACE ELECTRONIC STRUCTURE

Because the electronic eigenstates are represented in a plane-wave basis, the definition of surface states must be based on projections onto localized basis functions. For that purpose, the plane-wave basis functions of each state were expanded in terms of spherical waves inside spheres of radius 2.19 Å—corresponding to the assumed atomic radii—centered at the Co and Si atoms in the surface planes.[31] To be detected as a surface state the percentage of localization in the atomic spheres had to be at least 20%.

For the projection of bulk bands, eigenvalues were calculated for bulk geometries having the same stacking sequence as the corresponding slabs representing the surfaces. This was done for a sufficiently dense mesh of planes in **k** space orthogonal to the proper k_z direction. The projection is done as follows: if the difference between two eigenvalues for varying k_z coordinates for fixed (k_x,k_y) coordinates is smaller than 0.06 eV, then they are immersed in the shaded areas of Figs. 6(a), 6(b), 6(c). Otherwise, gaps exist in the projected bands. If new states occur in distinct gaps of the projected band structure, one can safely denote these states as surface states.

For the interpretation of selected surface states, charge density contours are shown in Figs. 7, 8, and 9. We calculate pseudocharge densities based on nodeless pseudoorbitals and localized augmentation functions.[12,11] Therefore, the nodal structure of the valence states in the region of the ionic cores is not reproduced.

A. Dispersion relations of surface states

1. (100)

As discussed above, the (100) stoichiometric slab has two different surfaces. Therefore, Fig. 6(a) shows surface states

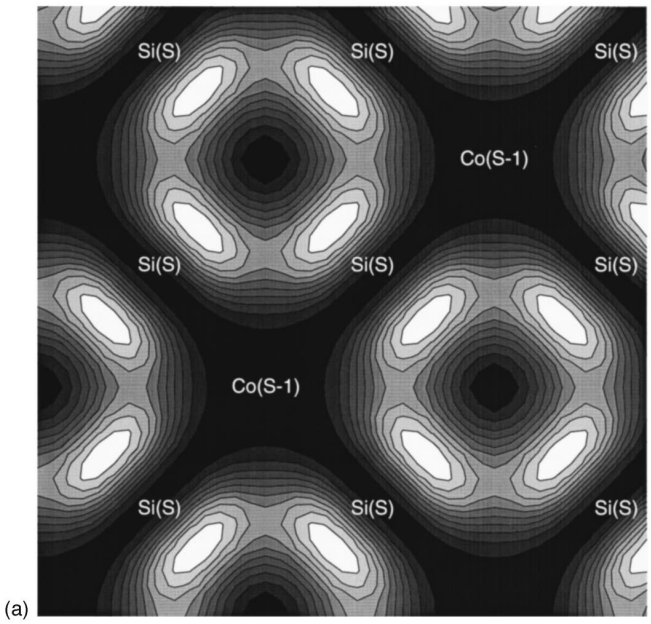

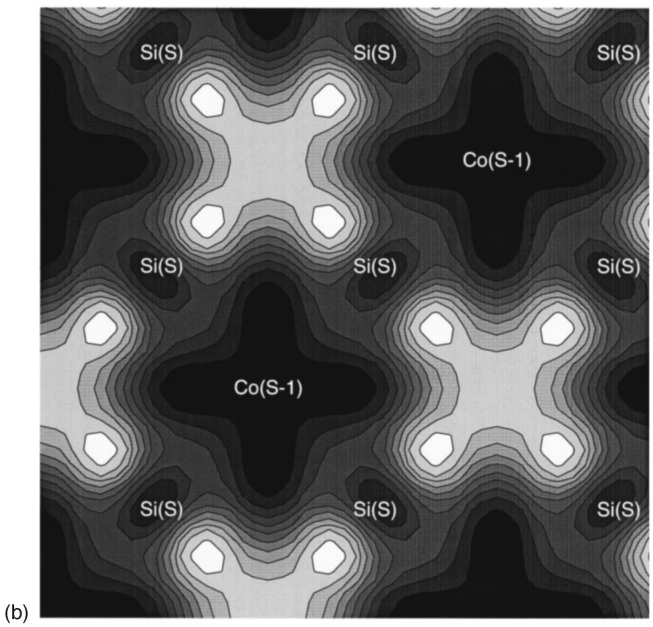

FIG. 7. Contour plots for the electronic densities of surface states for the Si-terminated (100) surface at $\overline{X}$. Plane through the atomic positions of top Si(S) (same cut as in Figs. 2–5 regarding the x and y coordinates). Subsurface layer atomic positions denoted by Co($S-1$). (a) state at 1.711 eV, (b) state at 1.716 eV.

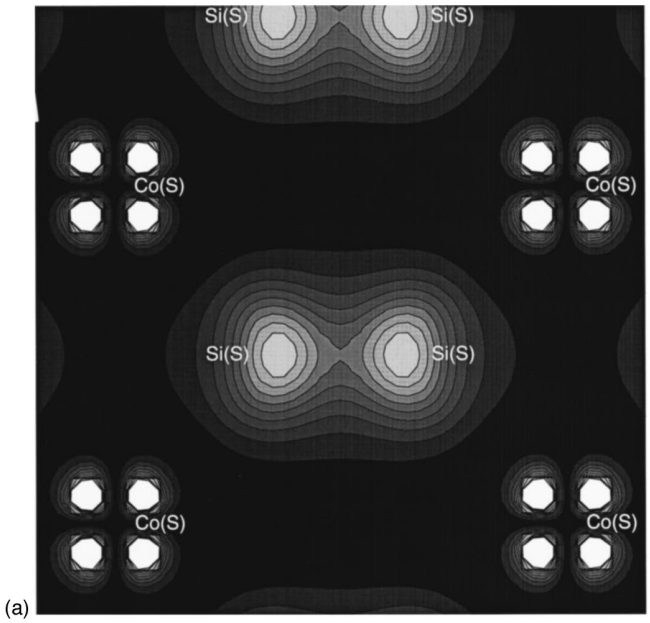

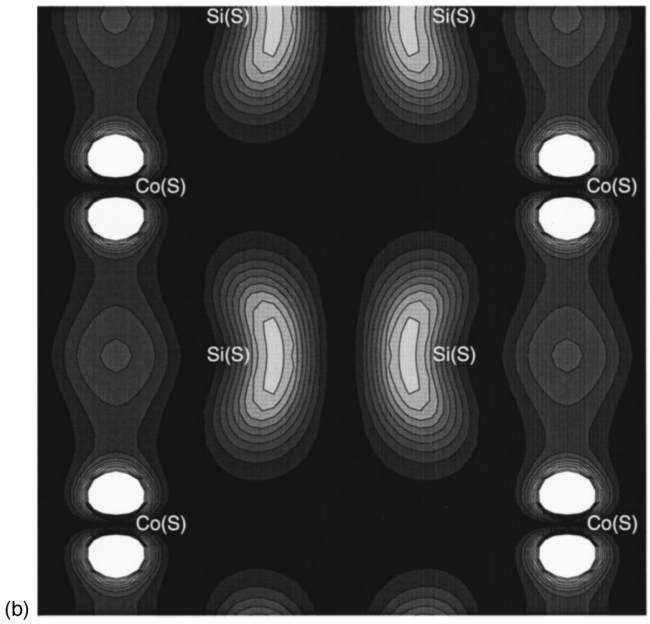

FIG. 8. Contour plots for the electronic densities of surface states for the (110) surface at $\overline{S}$ with energy (a) 0.022 eV below and (b) 1.754 eV above the Fermi energy. Cut through the atomic positions of Si in the surface plane where the rectangular two-dimensional elementary cell is formed by the Co positions in the top-layer of Fig. 1(c). Atomic positions denoted by Si and Co, both in the same surface layer but with slightly rumpled positions.

of both types of surfaces: the black dots for the Co-terminated surface, and the gray dots for the Si termination.

Noticeable surface states occur in the gap at $\overline{X}$ above Fermi energy. Strikingly, at $\overline{X}$ there seems to be a degeneracy of two states at 1.71 eV: from direction $\overline{\Gamma}$-$\overline{X}$ as well as from $\overline{M}$-$\overline{X}$ two bands merge at the same energy. A small energy difference of 0.005 eV, however, remains between the two states. Inspecting the nature of the states in the surface plane (Fig. 7) we found bonding features between Si-surface positions for both of them: whereas the slightly lower-lying state at 1.711 eV (state A) shows distinct p-p bonding features along the sides of the square formed by the Si surface atoms [Fig. 7(a)], the state at 1.716 eV (state B) reveals p orbitals directed along the diagonals of the square [Fig. 7(b)]. Whereas state B couples in a bonding manner to the subsurface Co atoms and even deeper to the next lower Si layers, state A is of antibonding character with respect to the Co-subsurface atoms: the Co bonds are rather localized in the subsurface plane with nodes between surface and subsurface layer.

For the Co-terminated surface, interactions of Co surface atoms with subsurface Si partners also create surface states

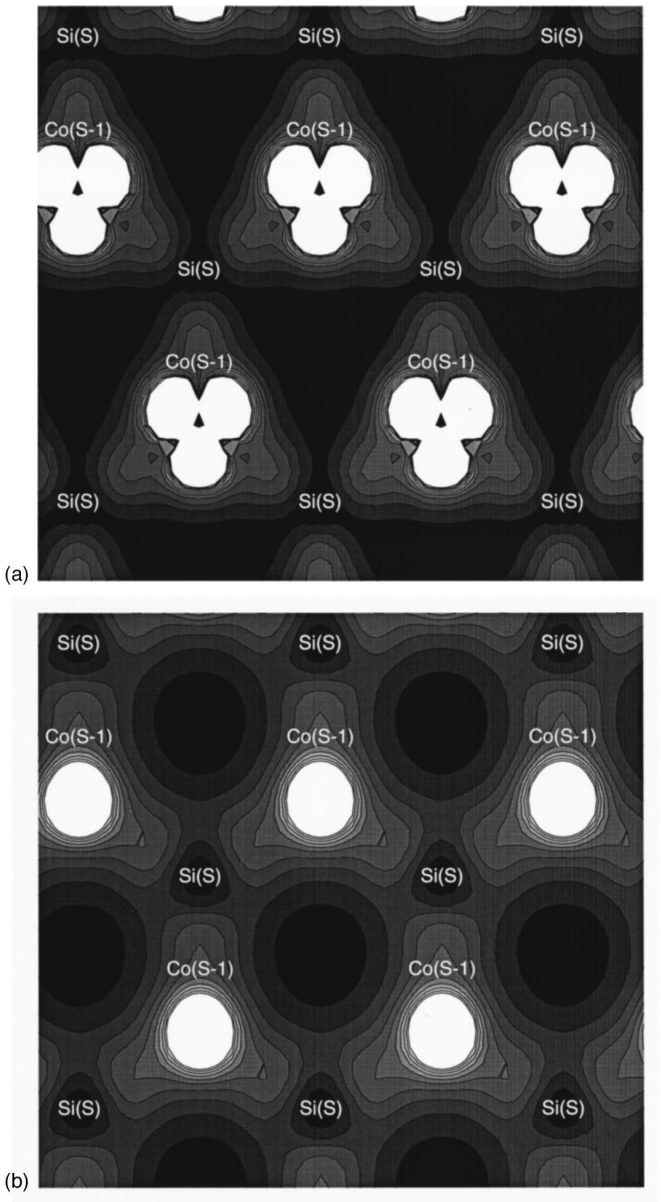

FIG. 9. Contour plots for the electronic densities of surface states for the (111) surface at $\overline{K}$ with energies (a) 1.292 eV below and (b) 0.220 eV above the Fermi energy. In surface plane, cut is made through the Si positions. Co of subsurface layer in center of triangular-shaped contours. The hexagonal two-dimensional elementary cell is formed by the Si positions in the top layer of Fig. 1(d).

as it is the case for the Co-surface state at 2.27 eV: d_{xz}- and d_{yz}-like Co orbitals couple strongly to Si-p_z orbitals. Because the formation of the Co-terminated surface removed some of the bonds to Si, such states are pushed up in energy in comparison to the corresponding bulk states.

Numerous surface localized Co-surface states are found in the bulk projected areas, which, however, are not always true surface states but rather localized *d* states that might also be found in the bulk.

2. (110)

As already discussed in Ref. 10, an appreciable number of surface states is found particularly at $\overline{X}$. Very good agreement is found with these FLAPW data conerning the position and nature of the states. However, in Ref. 10 the $\overline{S}$ point was not taken into account, at which also interesting surface states occur. Black and gray dots refer now to Co and Si atoms in the same layer (although a small corrugation effect is found after relaxation as discused in Sec. III B), and mark the predominant character [Fig. 6(b)].

The geometrical type of this surface is quite different from the other two cases because Co and Si atoms are situated in the same layer. For the other two orientations, the layers contain only either Si or Co. Due to the mixed atomic arrangement of the (110) layers, in-plane surface states with covalent Co-Si character are now possible. These states due to the (110) stacking also generally couple to the subsurface layer. Therefore, if (nearly) double degeneracy of surface states occurs, it is not due to the planar nature of the state, but due to the two equivalent surfaces of the slab. It can be realized from Fig. 6(b), that an observable splitting of some surface bands occurs: the corresponding states reach so deep down, that the chosen slab of seven layers is not sufficiently thick to perfectly decouple the surfaces.

At point $\overline{S}$ two high-symmetry directions parallel to the k_x and k_y axes cross, which makes any combinations of Co and Si orbitals parallel to the *x* and *y* axes possible, and the orbitals might be parallel or orthogonal to each other.

For example, strongly covalent in-plane *p*-*p* bonding between two Si positions and *p*-*d* bonding combinations between Co and Si is shown by Figs. 8(a) and 8(b), correspondingly, for the surface state at $\overline{S}$, 0.02 eV below [Fig. 8(a)] and 1.75 eV above [Fig. 8(b)] the Fermi energy.

Like in Fig. 6(a), many Co-localized states are found for which no true surface character can be claimed.

3. (111)

As discussed above, the termination of the investigated (111) surface consists of a trilayer Si-Co-Si with Si on the surface. Therefore, when properly stacked the second surface of the slab also has the same termination. No Co-like surface localized states are now possible, only gray dots are found in Fig. 6(c). In contrast to the other two surface orientations, which showed quite a richness of surface states, for the (111) surface in the main gap above the Fermi energy only two surface bands are present. These bands are doubly degenerate, because the surfaces of the slab are equal and the surface effects obviously well screened.

The threefold geometry is obviously rather favorable; the bonds between Co and Si are strong: the relaxation of the surface layer towards the Co plane by 0.10 Å is appreciable (Table IV). Concerning only the geometry, Co is ideally placed because it lies in a tetrahedral position [Fig. 1(d)]. Figure 9(a) shows contours of the state 1.29 eV below Fermi energy at $\overline{K}$ where the bulk projected area thins out to a single point, the state has presumably some bulklike character although localized in the Si-surface spheres. Quite a large accumulation of charge is seen between a triangle of Si atoms, for which its center lies above the Co position. The surface state at 0.22 eV above Fermi energy at $\overline{K}$ [Fig. 9(b)] is a weak resemblance of the strong bonding bulklike state. Weak bonding islands between the Co positions can also be observed. The second surface state at 1.00 eV above Fermi

energy is the antibonding counterpart of the state at 0.22 eV.

Distinct surface bands in bulk projected gaps are also found well below the Fermi level. For example, a band at -7.5 eV is found at $\overline{K}$ that crosses through the large gap at this point. At a similar energy, surface or resonant states are also seen for the (100) band structure at $\overline{X}$ and for the (110) case at $\overline{S}$ but they are hardly or even not split off the bulk projections.

B. Work functions

Due to the repeated slab construction, the reference of energy has to be chosen as the average of the Coulomb potential in the middle of the vacuum. Because the potential is not perfectly flat in this region, some uncertainty remains. Our predicted values for the work-functions are 4.6, 4.9, and 3.4 eV for the (100), (110), and (111) surface. The outstandingly small value for the (111) surface reflects the strong relaxation of the Si surface layer, which reduces the surface dipole. A recent FLAPW study for the (110) surface[10] reported a value of 5.24 eV for the work function. This calculation was performed within a free slab model, which provides a correct reference energy. Concerning the different values of work functions obtained by both methods one also has to note that the value of the present VASP calculation was derived within the GGA approximation in contrast to the FLAPW result based on LDA.

V. SUMMARY

The aim of our paper was to provide a fundamental understanding of the energetics, structure and bonding properties of the clean (100), (110) and (111) surfaces of $CoSi_2$. The cleavage energies for (100) and (110) surfaces are rather similar in contrast to the (111) case, which has a substantially lower value. Applying simple models this behavior is understood and described. By analyzing the electronic structure we found for the (100) and (110) surfaces a number of surface states of rather covalent character. For the (111) surface with Si-Co-Si termination, only two surface bands are found in the bulk gap above the Fermi energy. Based on energetical results as well as on calculated STM images, a proposed $\sqrt{2}\times\sqrt{2}$ reconstruction of the (100) surface can be ruled out.

ACKNOWLEDGMENTS

The work was supported by the Austrian Science Foundation (Project. No. P10645-PHY). Partial support provided by the Center for Computational Materials Science (CMS), the HCM-Program ''*Ab initio* (from electronic structure) calculation of complex processes in materials'' (Contract No. ERBCHRXCT930369) of the European Union, and the City of Vienna (Jubiläumsstiftung) is gratefully acknowledged. A major part of the calculations was performed on the systems of the Computing Center of the University of Vienna. We thank J. Redinger, D. Vogtenhuber, W. Wolf, and E. G. Moroni for valuable discussions. We are much indebted to G. Ritz and W. Hofer for STM advice.

[1] R. Tung, Mater. Chem. Phys. **32**, 107 (1992).
[2] H. Sirringhaus, E. Y. Lee, and H. von Känel, J. Vac. Sci. Technol. B **12**, 2629 (1994); P. Werner, W. Jäger, and A. Schüppen, J. Appl. Phys. **74**, 3846 (1993); and references therein.
[3] S. Mantl, Mater. Sci. Rep. **8**, 1 (1992).
[4] R. Stalder *et al.*, Surf. Sci. **271**, 355 (1992).
[5] Y. Zhou *et al.*, Phys. Rev. B **47**, 10 395 (1993).
[6] U. Starke *et al.*, Surf. Sci. **352-354**, 89 (1996); W. Weiss *et al.*, *ibid.* **347**, 117 (1996).
[7] U. Starke *et al.*, Surf. Rev. Lett. (to be published).
[8] J. M. Gallego *et al.*, Surf. Sci. **239**, 203 (1990).
[9] G. Castro *et al.*, Surf. Sci. **117**, 621 (1982).
[10] D. Vogtenhuber and R. Podloucky, Phys. Rev. B **55**, 10 805 (1997).
[11] G. Kresse and J. Hafner, Phys. Rev. B **48**, 13 115 (1993); **49**, 14 251 (1994); G. Kresse and J. Furthmüller, Comput. Mater. Sci. **6**, 15 (1996); Phys. Rev. B **54**, 11 169 (1996).
[12] D. Vanderbilt, Phys. Rev. B **41**, 7892 (1990).
[13] G. Kresse and J. Hafner, J. Phys.: Condens. Matter **6**, 8245 (1994).
[14] R. Stadler *et al.*, Phys. Rev. B **54**, 1729 (1996).
[15] A. Eichler, G. Kresse, and J. Hafner, Phys. Rev. Lett. **77**, 1119 (1996).
[16] E. G. Moroni *et al.*, Phys. Rev. B **56**, 15 629, (1997).
[17] S. G. Louie, S. Froyen, and M. L. Cohen, Phys. Rev. B **26**, 1738 (1982).
[18] H. J. Monkhorst and J. D. Pack, Phys. Rev. B **13**, 5188 (1976).
[19] M. Methfessel and A. T. Paxton, Phys. Rev. B **40**, 3616 (1989).
[20] A. D. Becke, Phys. Rev. A **38**, 3098 (1988); J. P. Perdew, Phys. Rev. B **33**, 8822 (1986).
[21] R. Stadler, Ph.D. thesis, University of Vienna (unpublished).
[22] C. Pirri, J. C. Peruchetti, D. Bolmont, and G. Gewinner, Phys. Rev. B **33**, 4108 (1986).
[23] F. Hellman and R. T. Tung, Phys. Rev. B **37**, 10 786 (1988).
[24] J. Vrijmoeth, A. G. Schins, and J. F. van der Veen, Phys. Rev. B **40**, 3121 (1989).
[25] D. D. Chambliss, T. N. Rhodin, and J. E. Rowe, Phys. Rev. B **45**, 1193 (1992).
[26] M. Methfessel *et al.*, Appl. Phys. A: Solids Surf. **55**, 444 (1992).
[27] J. Tersoff and D. R. Hamann, Phys. Rev. B **31**, 805 (1985).
[28] A. Biedermann (private communication).
[29] W. Hofer, Phys. Rev. Lett. (to be published).
[30] B. Voigtländer *et al.*, Phys. Rev. B **55**, R13 444 (1997).
[31] A. Eichler, G. Kresse, and J. Hafner, Surf. Sci. **346**, 300 (1995).